

HtrA2 deficiency causes mitochondrial uncoupling through the F₁F₀-ATP synthase and consequent ATP depletion

H Plun-Favreau^{*,1,7}, VS Burchell^{1,7}, KM Holmström¹, Z Yao^{1,2}, E Deas¹, K Cain³, V Fedele³, N Moiso³, M Campanella^{4,5}, L Miguel Martins³, NW Wood¹, AV Gourine⁶ and AY Abramov^{*,1}

Loss of the mitochondrial protease HtrA2 (Omi) in mice leads to mitochondrial dysfunction, neurodegeneration and premature death, but the mechanism underlying this pathology remains unclear. Using primary cultures from wild-type and HtrA2-knockout mice, we find that HtrA2 deficiency significantly reduces mitochondrial membrane potential in a range of cell types. This depolarisation was found to result from mitochondrial uncoupling, as mitochondrial respiration was increased in HtrA2-deficient cells and respiratory control ratio was dramatically reduced. HtrA2-knockout cells exhibit increased proton translocation through the ATP synthase, in combination with decreased ATP production and truncation of the F1 α -subunit, suggesting the ATP synthase as the source of the proton leak. Uncoupling in the HtrA2-deficient mice is accompanied by altered breathing pattern and, on a cellular level, ATP depletion and vulnerability to chemical ischaemia. We propose that this vulnerability may ultimately cause the neurodegeneration observed in these mice.

Cell Death and Disease (2012) 3, e335; doi:10.1038/cddis.2012.77; published online 28 June 2012

Subject Category: Internal Medicine

The serine protease HtrA2 was first identified as a pro-apoptotic protein that is released into the cytosol following opening of the mitochondrial permeability transition pore (reviewed in Vande Walle *et al.*¹). However, HtrA2-knockout (KO) mice demonstrate striatal neurodegeneration² and premature death, and mutations in the *HtrA2* gene have also been identified in German and Belgian Parkinson's disease (PD) patients,^{3,4} suggesting a role for the protein in neuroprotection. Mice lacking functional HtrA2 and cells derived from them show impaired mitochondrial function,^{2,5} and *Drosophila* lacking HtrA2 were found to exhibit increased numbers of defective mitochondria,⁶ all suggesting a crucial role for HtrA2 in maintaining mitochondrial physiology. We have therefore investigated the effect of HtrA2 deficiency on mitochondrial function using a combination of live microscopy and biochemical techniques. Here, we show that cells derived from HtrA2-KO mice exhibit decreased mitochondrial membrane potential ($\Delta\Psi_m$) but increased mitochondrial respiration, suggesting severe uncoupling of oxidative phosphorylation. They further show increased hyperpolarisation in response to oligomycin but decreased ATP production by the ATP synthase, suggesting that the proton leak occurs through the ATP synthase itself, indicating a novel role for HtrA2 in the

maintenance of this protein complex. This uncoupling in turn leads to an alteration in breathing pattern *in vivo*, cellular ATP depletion and an increased vulnerability to chemical ischaemia, which may underlie the neurodegeneration and premature mortality observed in HtrA2-KO animals.

Results

$\Delta\Psi_m$ is reduced in HtrA2-deficient cells. $\Delta\Psi_m$ is an important indicator of mitochondrial health. Using tetramethylrhodamine methylester (TMRM) as a fluorescent indicator of $\Delta\Psi_m$, we found that HtrA2 deficiency induced a significant decrease in basal $\Delta\Psi_m$ in all primary cell types studied (Figure 1a). Interestingly, this decrease was most significant in midbrain neurons, even compared with neighbouring astrocytes or cortical neurons from the same animals. Decreased $\Delta\Psi_m$ was observed not only in brain primary cultures, but also in primary myocytes from HtrA2-deficient animals (Figure 1a), and in other models such as immortalised mouse embryonic fibroblasts (MEFs) (data not shown). Therefore, HtrA2 is likely to be essential for healthy mitochondrial function in multiple tissues, particularly in midbrain neurons.

¹Department of Molecular Neuroscience, UCL Institute of Neurology, Queen Square, London WC1N 3BG, UK; ²Department of Cell and Developmental Biology, Consortium for Mitochondrial Research, University College London, Gower Street, London WC1E 6BT, UK; ³Cell Death Regulation Laboratory, MRC Toxicology Unit, Leicester LE1 9HN, UK; ⁴Royal Veterinary College, University of London, London NW1 0TU, UK; ⁵Metabolism in Brain Diseases Unit, EBRI Foundation, Rome, Italy and ⁶Department of Neuroscience, Pharmacology and Physiology, University College London, Gower Street, London WC1E 6BT, UK

*Corresponding author: AY Abramov or H Plun-Favreau, Department of Molecular Neuroscience, UCL Institute of Neurology, Queen Square, London WC1N 3BG, UK. Tel: +44 2078 3736 11; Fax: +44 2072 785 616; E-mail: a.abramov@ucl.ac.uk (AYA) or h.plun-favreau@ion.ucl.ac.uk (HPF)

⁷These authors contributed equally to this work.

Keywords: HtrA2; mitochondria; uncoupling; ATP synthase

Abbreviations: $\Delta\Psi_m$, mitochondrial membrane potential; PD, Parkinson's Disease; MEFs, mouse embryonic fibroblasts; KO, knockout; WT, wild type; ROS, reactive oxygen species; UCP, mitochondrial uncoupling protein; RCR, respiratory control ratio

Received 15.5.12; accepted 16.5.12; Edited by G Melino

In healthy cells, $\Delta\Psi_m$ is maintained by the activity of the mitochondrial respiratory chain. In the event of damage or inhibition of respiration, cells may maintain $\Delta\Psi_m$ using ATP hydrolysis by the ATP synthase (reviewed in Nicholls *et al.*⁷). In order to investigate the mechanism of maintenance of $\Delta\Psi_m$, we applied a series of mitochondrial toxins and observed their effects on $\Delta\Psi_m$.^{8,9} In wild-type (WT) midbrain neurons, application of oligomycin (2 $\mu\text{g}/\text{ml}$), an inhibitor of the F_1F_0 -ATPase, induced no response or a slight hyperpolarisation as proton entry through the ATP synthase was inhibited. Application of rotenone (5 μM) to inhibit complex I then produced a profound depolarisation, and complete depolarisation was estimated by addition of the mitochondrial uncoupler FCCP (1 μM ; Figure 1c). This indicates that in WT midbrain neurons most of the $\Delta\Psi_m$ is maintained by the

respiratory chain. In HtrA2-KO midbrain neurons, application of oligomycin also induced hyperpolarisation (Figure 1d), indicating that the $\Delta\Psi_m$ is still maintained by the mitochondrial respiratory chain and suggesting that, even under conditions of very low $\Delta\Psi_m$, the ATP synthase in HtrA2-deficient neurons and astrocytes is unable to switch to hydrolysis mode. Interestingly, this hyperpolarisation in response to oligomycin was significantly greater in HtrA2-KO cells (Figures 1b and d) than in cells from WT littermates (Figure 1c). This indicates that proton entry into the mitochondrial matrix through the ATP synthase is in fact increased in HtrA2-KO cells compared with WT, despite the lower $\Delta\Psi_m$.

Mitochondrial respiration is increased in HtrA2-deficient cells. There are several possible explanations for a

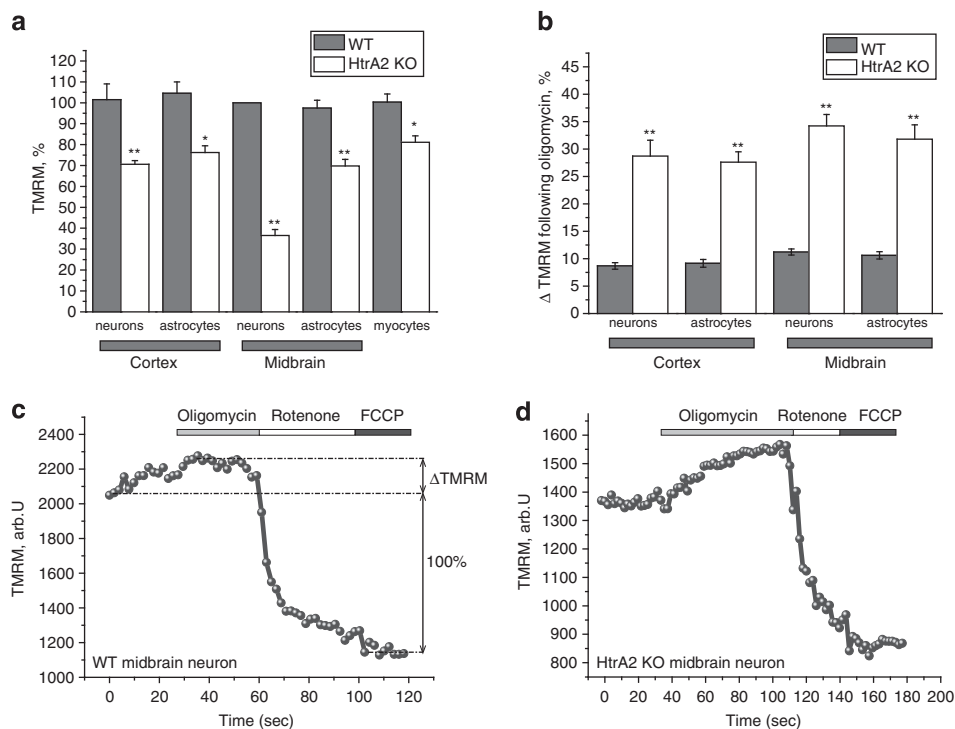
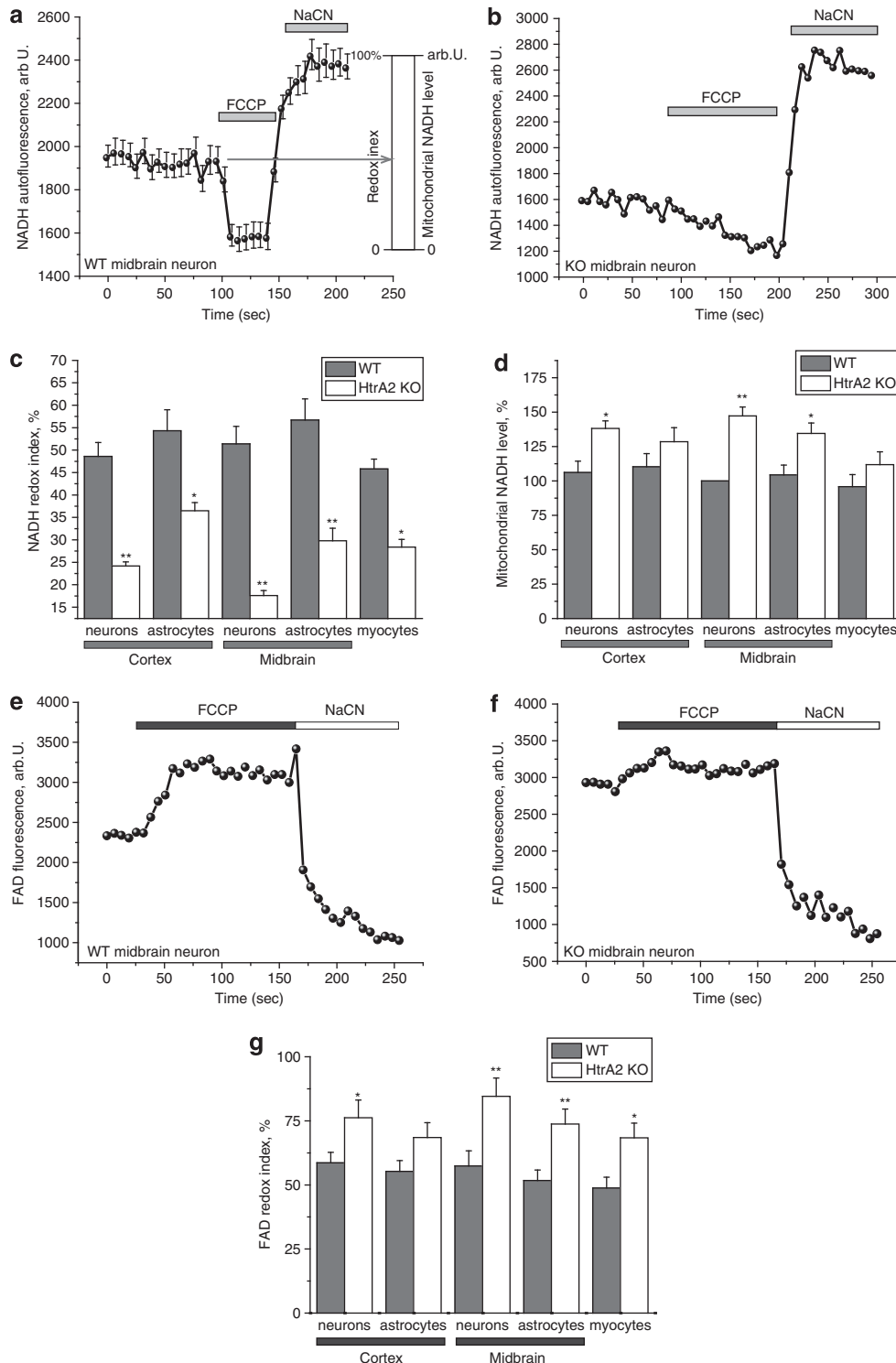


Figure 1 Mitochondria are depolarised in HtrA2-deficient cells. (a) Mitochondrial membrane potential was estimated by live cell imaging in a range of primary cell types using TMRM in redistribution mode (25 nM). Data are normalised to midbrain astrocytes (100%) and are represented as mean \pm S.E.M. (b) Mitochondrial hyperpolarisation (ΔTMRM) in response to oligomycin (2 $\mu\text{g}/\text{ml}$) is presented as a percentage of the difference between the initial TMRM fluorescence and the minimum TMRM fluorescence achieved after addition of FCCP (1 μM ; see Figure 1c). (c and d) Representative TMRM traces for one WT (c) and one KO (d) midbrain neuron, showing responses to oligomycin (2 $\mu\text{g}/\text{ml}$), rotenone (5 μM) and FCCP (1 μM). In all cases, * indicates $P < 0.05$ and ** indicates $P < 0.01$ compared with WT values

Figure 2 Mitochondrial respiration is increased in HtrA2-deficient cells. (a) NADH autofluorescence was monitored in WT midbrain neurons by confocal microscopy. Addition of the uncoupler FCCP (1 μM) maximises mitochondrial respiration and thereby minimises mitochondrial NADH. NaCN (1 mM) was then added to block mitochondrial respiration and therefore maximise mitochondrial NADH. Redox index (the initial redox level expressed as a percentage of the range) and mitochondrial NADH level (the difference in absolute values between the minimum and maximum NADH autofluorescence) are described graphically. Data are represented as the mean of several cells on a single coverslip \pm S.E.M. (b) A representative trace is shown for a single HtrA2-KO midbrain neuron, demonstrating the smaller response to FCCP and larger response to NaCN in this cell compared with the WT (Figure 2a). (c) NADH redox index was calculated for a variety of primary cell types by calculating the initial NADH autofluorescence when the minimum NADH autofluorescence is normalised to 0% and the maximum to 100%. NADH redox index was reduced in all HtrA2-KO cell types but particularly in midbrain neurons. Data are represented as mean \pm S.E.M. (d) Mitochondrial NADH level was calculated as the difference in arbitrary units between the maximum and minimum NADH autofluorescence. Data were normalised to midbrain astrocytes (100%) and represented as mean \pm S.E.M. (e and f) FAD autofluorescence was monitored by confocal microscopy in WT (e) and HtrA2 KO (f) midbrain neurons. Addition of FCCP (1 μM) maximised respiration and therefore increased FAD autofluorescence to maximal levels. Addition of NaCN (1 mM) then inhibited respiration and reduced FAD autofluorescence to a minimum. Data shown are representative traces from single midbrain neurons. (g) FAD redox index was calculated for a range of primary cell types by normalising the FCCP response to 100% and the NaCN response to 0%. Data are represented as mean \pm S.E.M. In all cases, * indicates $P < 0.05$ and ** indicates $P < 0.01$ compared with WT values

reduction in $\Delta\Psi_m$, including damage to the mitochondrial respiratory chain or uncoupling of oxidative phosphorylation. In order to investigate mitochondrial respiration specifically in either neurons or astrocytes, we measured NADH autofluorescence in co-cultures of primary neurons and astrocytes and calculated the redox index. NADH is the electron donor for complex I, and as such, NADH levels correlate inversely

with respiratory chain activity. In order to measure redox index, we added FCCP ($1\ \mu\text{M}$) to maximise respiration and therefore minimise the NADH pool, then added NaCN ($1\ \text{mM}$) to block mitochondrial respiration and therefore maximise the NADH pool. The initial NADH autofluorescence is then calculated as a percentage of this range (Figure 2a). In addition, the total mitochondrial pool of NADH (maximum



autofluorescence minus minimum) may be taken as an indication of the substrate availability for complex I.

We observed a significant decrease in redox level in HtrA2-deficient neurons, astrocytes and myocytes, indicating increased respiration rate in these cells (Figures 2b and c). Importantly, the lowest redox index was again observed in midbrain neurons (Figure 2b), correlating with the low $\Delta\Psi_m$ in these cells. The total mitochondrial pool of NADH in HtrA2-KO cells was also significantly higher than in WT, indicating increased substrate availability in these cells (Figure 2d).

Activity of complex II can similarly be estimated by measuring autofluorescence of flavoproteins,¹⁰ as FAD(H₂) is the redox cofactor for complex II. We examined FAD⁺⁺ autofluorescence in primary co-cultures of midbrain or cortical neurons and astrocytes. FAD⁺⁺ redox level was estimated in the same way as NADH, but in this case the response to NaCN was taken as 0% and response to FCCP as 100%. In agreement with our NADH data, application of FCCP to KO midbrain neurons induced only a mild increase in FAD⁺⁺, but application of NaCN to these cells induced a massive decrease in autofluorescence (Figure 2e), indicating that mitochondrial respiration in these cells is close to maximal.

Oxygen consumption is increased in HtrA2-deficient cells. The finding that mitochondrial respiration is increased in HtrA2-deficient cells was confirmed in immortalised HtrA2-KO and WT MEFs using a Clark oxygen electrode (Figure 3a). We observed that basal oxygen consumption was significantly increased in the HtrA2-KO cells compared

with control cells. Oligomycin (2 μ g/ml) inhibited the respiration coupled to oxidative phosphorylation in control cells but to a significantly lesser extent in HtrA2-KO cells. Addition of 1 μ M of the uncoupler FCCP accelerated respiration to maximal levels in both control and HtrA2-KO cells, suggesting that this effect is not induced by overexpression of mitochondrial complexes in these cells.

In order to investigate this effect in detail, we used isolated mitochondria from the brains of WT and HtrA2-KO animals. We found that HtrA2 deficiency leads to significantly increased oxygen consumption in state 3 respiration, whether using substrates for complex I (5 mM glutamate and 5 mM malate) or substrates for complex II (5 mM succinate in the presence of rotenone; Figure 3b). The difference in rates of respiration between HtrA2-WT and KO mitochondria was even higher in state 4 respiration (without ADP stimulation; Figure 3c). Respiratory control ratio (RCR) is the ratio of state 3 respiration (ADP stimulated) to state 4 respiration (no ADP present), and is considered an indication of the degree of coupling of mitochondrial respiratory chain activity to oxidative phosphorylation.¹⁰ The RCR was significantly lower in HtrA2-KO cells than in WT cells (Figure 3b). These data demonstrate severe mitochondrial uncoupling in HtrA2-deficient cells, explaining the decreased $\Delta\Psi_m$ but increased rate of mitochondrial respiration.

Mitochondrial reactive oxygen species production is reduced in HtrA2-deficient cells. The rate of mitochondrial reactive oxygen species (ROS) production is dependent on the value of $\Delta\Psi_m$, and uncoupling of mitochondrial oxidative

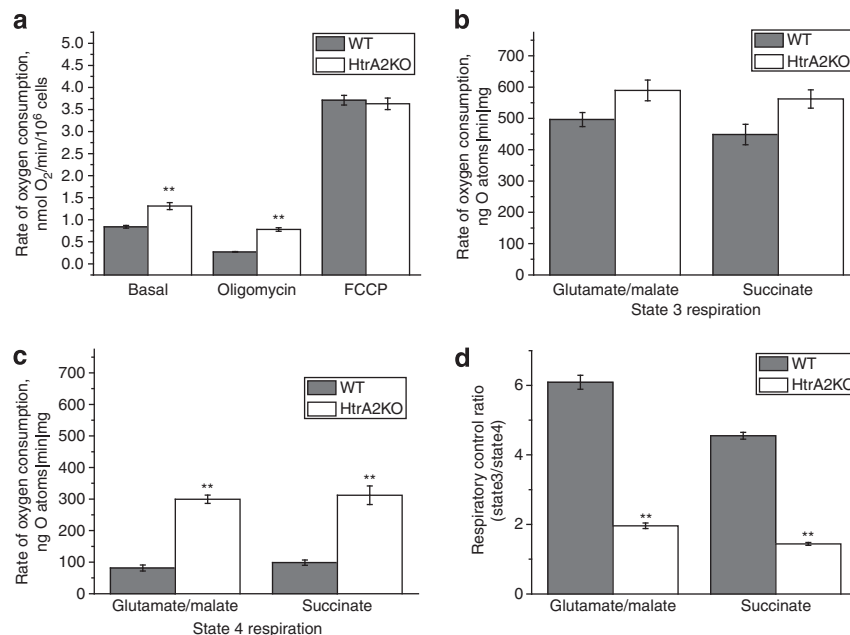


Figure 3 Oxygen consumption is increased in HtrA2-deficient cells. (a) Oxygen consumption was measured in whole immortalised MEFs using a Clark oxygen electrode. Respiration was inhibited by blocking ATP production using oligomycin (2 μ g/ml), and maximised by adding the uncoupler FCCP (1 μ M). (b and c) Whole mitochondria were isolated from the brains of WT and HtrA2-KO mice and oxygen consumption was measured in state III (in which ADP is provided and respiration is coupled to oxidative phosphorylation), (b) and state IV (in which no ADP is present), (c). The experiment was performed in the presence of substrates for complex I (5 mM glutamate and 5 mM malate) or substrates for complex II (5 mM succinate in the presence of 5 μ M rotenone). (d) RCR (ratio of state III to state IV respiration) was significantly reduced in mitochondria from the brains of HtrA2-KO mice compared with WT. Data is represented as mean \pm S.E.M. In all cases, * indicates $P < 0.05$ and ** indicates $P < 0.01$ compared with WT values

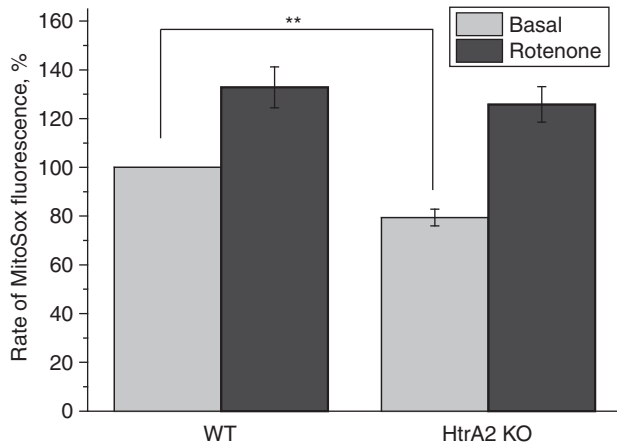


Figure 4 Mitochondrial ROS production is decreased in HtrA2-deficient cells. WT and HtrA2-KO midbrain cultures were loaded with MitoSOX (5 μ M), an indicator of mitochondrial ROS production, and monitored by fluorescence microscopy. The rate of increase in MitoSOX fluorescence (indicating mROS production) was significantly reduced in HtrA2-KO cells compared with WT. Neurons of both genotypes responded equally to stimulation of ROS production using rotenone (5 μ M). Data are represented as mean \pm S.E.M. ** Indicates $P < 0.05$

phosphorylation by FCCP has been shown to lead to a decrease in mitochondrial ROS production.¹¹ Using a mitochondrially targeted indicator of ROS, MitoSOX, we found that the basal level of mitochondrial ROS production in HtrA2-deficient neurons was significantly lower than in WT cells (Figure 4), consistent with mitochondrial uncoupling. The application of rotenone (5 μ M) inhibited complex I and accelerated the rate of mitochondrial ROS production in both WT and HtrA2-KO neurons to the same maximal rate, suggesting that the reduced rate of ROS production in HtrA2-deficient cells is not the result of reduced mitochondrial respiration.

ATP production by the F_1F_0 -ATP synthase is reduced in HtrA2-deficient cells. Following our observation that the hyperpolarisation in response to oligomycin is significantly higher in primary neurons from HtrA2-KO mice than WT (Figure 1d), we hypothesised that the mitochondrial uncoupling might occur through the ATP synthase itself. In order to investigate ATP production by the F_1F_0 -ATP synthase, we transfected cells with cytosolic luciferase¹² and perfused with 5 μ M luciferin. Addition of 1 mM ATP to the cells induced calcium uptake into the mitochondria, which stimulates mitochondrial respiration and consequently increased mitochondrial ATP production.¹³ This increase in ATP production was found to be significantly reduced in HtrA2-KO MEFs compared with WT (Figures 5a and b). This indicates that although proton translocation through the ATP synthase is increased in HtrA2-KO cells (indicated by hyperpolarisation in response to oligomycin), ATP production by the synthase is reduced, consistent with a possible leak of protons through the pore of the F_1F_0 -ATP synthase. The same result was also found in SH-SY5Y neuroblastoma cells in which HtrA2 was silenced by shRNA (Supplementary Figure 1).

To investigate this further, we assessed whether HtrA2 could interact with the ATP synthase. Tandem affinity purification (TAP) of HtrA2 from HEK cells overexpressing

HtrA2-TAP or the TAP tag (as a control) revealed an interaction between HtrA2 and the F1 α -subunit (Figures 5c and d). Furthermore, a proteomic analysis of mitochondria isolated from WT and HtrA2-KO liver revealed an alteration in this protein in KO mitochondria. When proteins were separated by 2D electrophoresis, an additional peak appeared in the HtrA2-KO sample at 41 kDa, which was not present in the WT (Figure 5e). This peak was identified by mass spectrometry as a truncated form of the α -subunit, lacking approximately 20 kDa at the N-terminus of the protein including the mitochondrial targeting sequence (MTS; Figure 5c). In order to exclude the possibility that this truncation could occur through alternative splicing, RNA was extracted from WT and HtrA2-KO brain tissue and quantitative real-time PCR was performed using primer pairs designed across each exon boundary of the *ATP5A1* gene, encoding the α -subunit (Supplementary Figure 2). A modest upregulation of *ATP5A1* was observed in HtrA2-KO tissue, but this relative increase in mRNA level was constant throughout the gene, with no evidence of the specific reduction in expression of one or more exons characteristic of alternative splicing (single factor ANOVA, $F = 0.37$, $P = 0.95$).

We additionally investigated any possible difference in UCP2 protein levels by western blot using two different antibodies. No difference was observed between WT and KO immortalised MEFs lysates, nor between WT and KO midbrain or cortex (data not shown).

HtrA2 deficiency reduces ATP levels and increases vulnerability to chemical ischaemia.

We next investigated the effect of mitochondrial uncoupling on cellular ATP levels and cell viability. Mag-Fura is a fluorescent indicator of divalent cations, with a high affinity for magnesium and a much lower affinity for calcium. As such, it can be used both to investigate ATP levels in individual cells, as ATP binds magnesium and, therefore, ATP levels are inversely proportional to free magnesium,¹⁴ and to investigate cytotoxicity in response to ATP depletion, as under these conditions the cell is no longer able to maintain its ionic homeostasis and floods with calcium.¹⁵ A sharp rise in Mag-Fura ratio therefore represents bioenergetic collapse. In HtrA2-KO midbrain neurons, we found that basal Mag-Fura ratio (ratio of magnesium-bound to free Mag-Fura) was significantly higher than in WT cells (Figures 6a and b), indicating lower ATP levels in these cells. Furthermore, following addition of 1 mM NaCN to block mitochondrial respiration, the Mag-Fura ratio was found to sharply increase after considerably less time in HtrA2-KO cells than in WT cells (Figures 6a and c). This indicates that HtrA2-KO cells are more vulnerable than WT to bioenergetic collapse in response to chemical ischaemia.

Breathing activity is altered in HtrA2-deficient mice.

Finally, we investigated whether the mitochondrial uncoupling observed in HtrA2-deficient mice is associated with increased respiratory effort *in vivo*. Surprisingly, we found that under resting conditions (normoxia/normocapnia) ventilation (V_E) was significantly lower in the KO mice (aged P20) in comparison with that of the WT or heterozygote counterparts ($P < 0.05$; Figure 7c). This difference arose

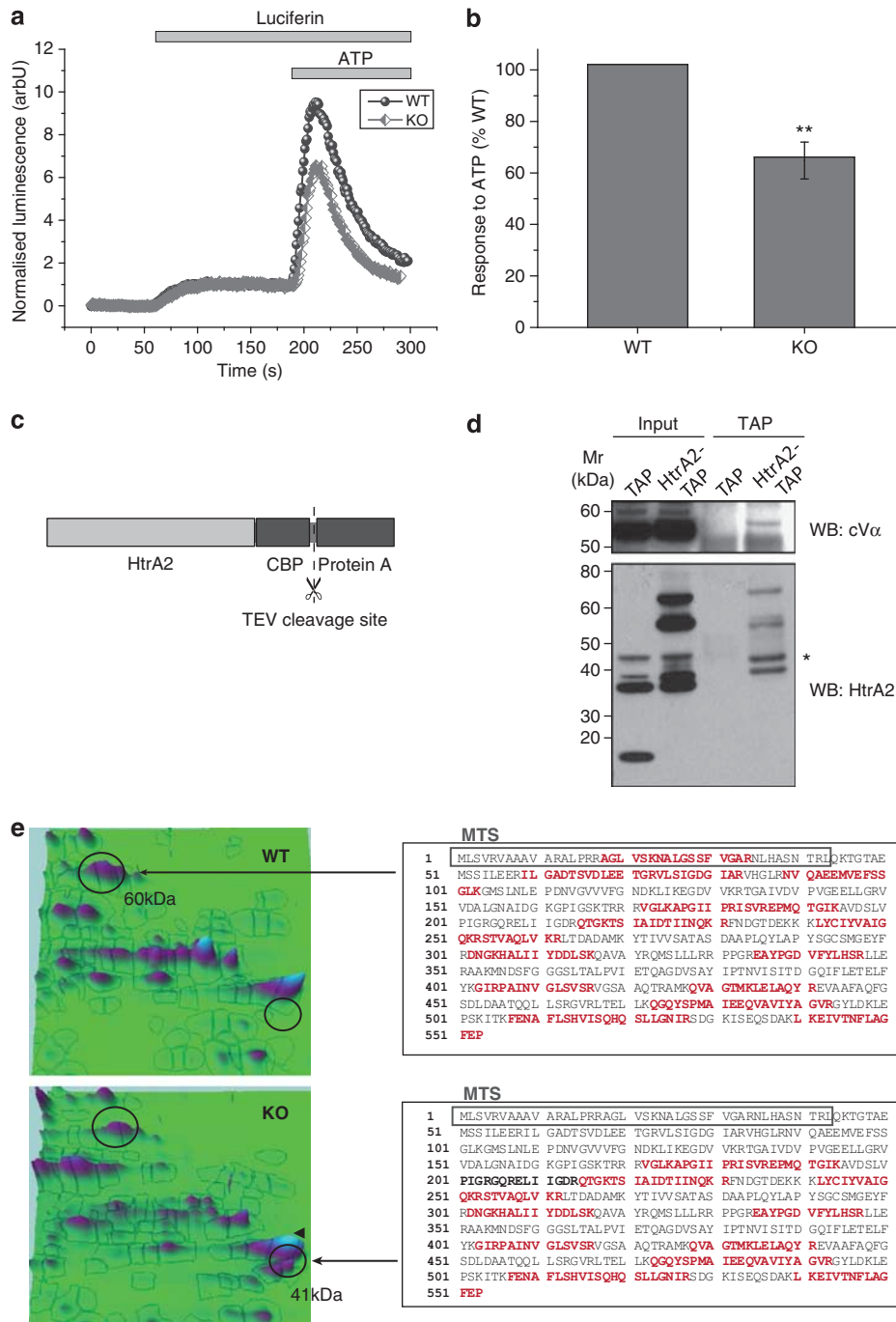


Figure 5 The F_1F_0 -ATP synthase is compromised in HtrA2-deficient cells. **(a)** ATP production was measured in live cells using a luciferin/luciferase based reporter assay. Immortalised MEFs transfected with cytosolic luciferase were perfused with luciferin ($5 \mu\text{M}$) followed by ATP (1 mM), which stimulates calcium uptake into mitochondria and therefore ATP production by the ATP synthase. Representative traces are shown for one WT and one KO coverslip. Initial luminescence is normalised to 0 and response to luciferin is normalised to 1. **(b)** ATP response curves were normalised to luciferin response as described, then for each pair of WT and KO coverslips the KO response was expressed as a percentage of the WT. Data are represented as mean \pm S.E.M. ** indicates $P < 0.01$ compared with WT. **(c)** HtrA2 was tagged at the C terminus with a TAP tag consisting of a protein A sequence (for IP with IgG beads) and a calmodulin binding peptide (CBP) sequence (for IP with calmodulin resin) separated by a TEV cleavage site. **(d)** The $F_1 \alpha$ -subunit (cV α) was identified in TAP eluates from HtrA2-TAP cells but not from TAP control cells. WB for HtrA2 shows endogenous processed HtrA2 (37 kDa) in TAP and HtrA2-TAP inputs, full-length and processed TAP-tagged HtrA2 (58 and 69 kDa) in the HtrA2-TAP inputs, and CBP-tagged processed HtrA2 (42 kDa) in the final eluate. * indicates a non-specific band. **(e)** A 2D-PAGE analysis of protein expression in WT and HtrA2-KO MEFs indicated a significant reduction in the peak corresponding to the α -subunit of the ATP synthase (60 kDa), and the appearance of a further peak identified by mass spectrometry as a truncated form of this subunit (41 kDa). The identified fragments are highlighted on the full length sequence of the α -subunit in red. In the truncated subunit good sequence coverage was obtained for the C-terminus but not the N-terminus of the protein, suggesting that truncation may remove the MTS (grey box)

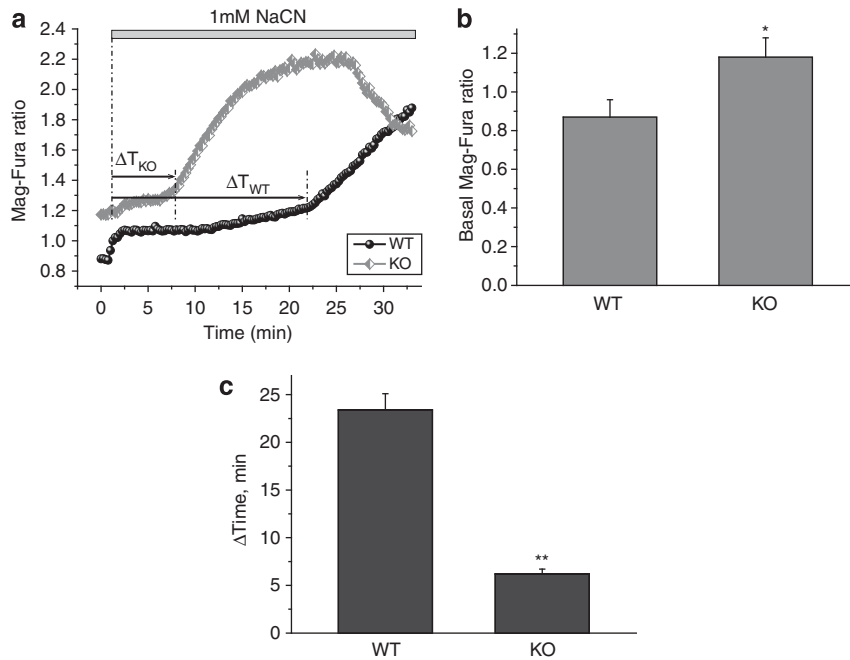


Figure 6 HtrA2 deficiency leads to ATP depletion and vulnerability to chemical ischaemia. (a–c) ATP levels were assessed indirectly using an indicator of free magnesium, Mag-Fura ($5 \mu\text{M}$). (a) shows representative traces for one WT and one HtrA2-KO midbrain neuron. Initial Mag-Fura ratio was significantly higher in HtrA2 KO traces than in WT (quantified in (b), data represented as mean \pm S.E.M.), indicating lower ATP levels in these cells. Inhibition of mitochondrial respiration by NaCN (1 mM) causes a slow increase in Mag-Fura ratio as ATP levels are depleted, followed by a sudden increase in Mag-Fura ratio as ATP levels are insufficient to maintain ionic homeostasis and the cell floods with calcium. The time to onset of this bioenergetic collapse is significantly shorter in the HtrA2-KO neurons compared with WT (quantified in (c), data represented as mean \pm S.E.M.), indicating increased vulnerability to chemical ischaemia. * Indicates $P < 0.05$, ** indicates $P < 0.01$.

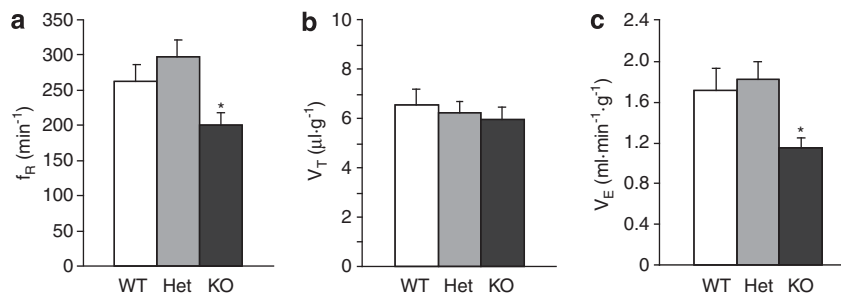


Figure 7 Whole animal respiration is reduced in HtrA2-deficient mice. Respiratory rate (f_R) and tidal volume (V_T) were assessed by whole-body plethysmography in conscious WT, heterozygous and HtrA2-KO mice aged P20. (a–c) Respiratory rate (a) was reduced in HtrA2-KO mice compared with their WT and heterozygous counterparts, but tidal volume (b) was unchanged. Minute ventilation (V_E), calculated as the product of f_R and V_T , was therefore significantly reduced in HtrA2-KO animals (c). Data are represented as mean \pm S.E.M., * indicates $P < 0.05$

from a significantly lower resting respiratory rate (f_R) but not tidal volume (V_T) in the KO mice (Figures 7a and b). Thus, mitochondrial uncoupling in HtrA2-deficient mice is accompanied by markedly reduced respiratory effort, which may contribute to the premature mortality in these transgenic animals.

Discussion

Previous work on HtrA2 has described a duality in its function: when released from the mitochondria in response to a death stimulus it has a pro-apoptotic role (reviewed in Vande Walle *et al.*¹), but while residing in the mitochondria it has an important neuroprotective role evidenced by the neuronal death in the KO mouse² and the *mnd2* mouse, which carries a mutation in

HtrA2 that inactivates its protease activity.¹⁶ Loss of HtrA2 has been shown to result in low $\Delta\Psi_m$ ⁵ and abnormal mitochondrial morphology and ultrastructure.^{2,5} In addition to mammalian systems, HtrA2-KO flies have also been found to display a progressive locomotor defect, and were also found to have increased numbers of defective mitochondria.⁶

In this study, we confirm the low $\Delta\Psi_m$ previously described in immortalised HtrA2-KO cells⁵ in primary neurons, astrocytes and myocytes. Strikingly, the $\Delta\Psi_m$ was lowest in midbrain neurons, even compared with cortical neurons. This region-specific phenotype is particularly interesting as it is the midbrain neurons, which are specifically affected in PD, linking the mitochondrial phenotype to the parkinsonian behavioural phenotype observed in these mice. The reason for this specificity is not clear but it is unlikely to be due to the

dopaminergic nature of midbrain neurons as only a small proportion are TH-positive (data not shown). One possibility is that differences in the expression profiles of neurons in the two brain regions may account for some of the difference.

In combination with low $\Delta\Psi_m$ we observed increased oxygen consumption in both whole cells and isolated mitochondria, indicating severe uncoupling of oxidative phosphorylation from proton translocation across the inner mitochondrial membrane. We find that this uncoupling leads to significant stimulation of cellular respiration and reduction in RCR. Using NADH/FAD redox levels to confirm this on a single-cell level, we found that mitochondrial respiration was most increased in midbrain neurons, following the same pattern as $\Delta\Psi_m$. This suggests that the uncoupling is most severe in these neurons.

We next sought to identify how loss of HtrA2 might lead to mitochondrial uncoupling. HtrA2 is a protease and so an attractive possibility could be that it is responsible for the turnover of mitochondrial uncoupling proteins (UCPs). These proteins are expressed in response to oxidative stress in order to reduce mitochondrial ROS production, but are rapidly degraded by an unknown mechanism. Western blot analysis did not reveal any difference in expression of UCP2 in HtrA2-KO brain lysates compared with WT brain. Instead, a surprising response of $\Delta\Psi_m$ to oligomycin suggested that there could be a functional alteration in the F_1F_0 -ATP synthase. The ATP synthase is able to work in two directions: under normal conditions it harnesses the translocation of protons into the mitochondrial matrix in order to catalyse the synthesis of ATP, but under conditions of low $\Delta\Psi_m$ it acts in reverse, hydrolysing ATP in order to pump protons out of the mitochondria and thereby maintain a sufficiently high $\Delta\Psi_m$ to prevent the mitochondrial permeability transition (reviewed in Nicholls *et al.*⁷). $\Delta\Psi_m$ in HtrA2-KO midbrain neurons is extremely low and so it would be expected that the ATP synthase would act in its reverse mode, in which case addition of oligomycin to block the ATP synthase would result in depolarisation.¹⁷ In fact, we observed the opposite: a significant increase in hyperpolarisation in response to oligomycin, indicating that more protons are entering the mitochondria through the ATP synthase in the KO cells than in the WT. This increase in proton translocation does not reflect an increase in ATP production, as ATP production by the ATP synthase in response to extracellular ATP was significantly reduced in HtrA2-KO cells compared with WT.

The mammalian ATP synthase is a complex of over 20 subunits and is the most abundantly expressed enzyme of the mitochondrial inner membrane. Despite this complexity, very few external regulators of the ATP synthase have been identified. In this study we find that HtrA2 interacts with the ATP synthase under basal conditions, and that a truncated form of the α -subunit of the synthase appears in isolated HtrA2-KO liver mitochondria. Although this was not the only protein identified as missing or significantly reduced in the HtrA2-KO mitochondria (spots corresponding to GR78, GR75, CH60 and SCB2 were also reduced), it was the only protein for which a cleavage product was identified and the most likely candidate to explain the observed phenotype. The α -subunit is a critical subunit of the ATP synthase as three α -subunits alternate with three β -subunits to form the ring

through which the central stalk of the ATP synthase rotates. This rotation causes the catalytic sites located on the β -subunits to undergo conformational changes that result in addition of inorganic phosphate to ADP. It is tempting to speculate, therefore, that alterations in this subunit could lead to a loosening of the structure, which could allow protons to pass through the pore of the synthase without the consequent rotation being harnessed to produce ATP. Some precedent has been shown for this in the literature: work in *Escherichia coli* has shown that a number of mutations in the ATP synthase lead to intrinsic mitochondrial uncoupling by affecting subunit interactions in the F1 domain,^{18,19} while in mammalian cells a mutation in subunit 6 of the ATP synthase known to cause Leber's hereditary optic neuropathy was shown to result in a proton leak through the ATP synthase.²⁰ Interestingly ATP6 mutations have also been shown to alter cristae formation in *Drosophila* cells,²¹ providing a link between alterations in the ATP synthase and alterations in mitochondrial ultrastructure such as those reported in HtrA2-deficient cells.^{2,5}

We additionally looked at the physiological consequences of this mitochondrial uncoupling *in vivo* by measuring whole animal respiration in mice aged P20, shortly before the onset of the behavioural phenotype. This time point reflects the previous mitochondrial physiology experiments, all of which were performed either in cells or mitochondria isolated from presymptomatic mice. Mitochondria isolated from older HtrA2-KO mice have previously been found to have impaired respiration,²² which may occur later in life, explaining the discrepancy. Surprisingly, *in vivo* ventilation was decreased despite the increased mitochondrial respiration observed in mitochondria isolated from KO mice at the same age. This combination of a reduction in oxygen supply coupled with an increase in oxygen consumption may contribute to the pathology in these animals in later life.

A major remaining question is how the loss of HtrA2 leads to truncation of the α -subunit. HtrA2 has been suggested to act as part of a mitochondrial protein quality control mechanism by degrading misfolded proteins not cleared by the proteasome,²³ and loss of HtrA2 has been shown to lead to an accumulation of misfolded proteins at the mitochondria, oxidative stress and activation of the integrated stress response.²² One possibility is, therefore, that the loss of this protein quality control mechanism could account for the occurrence of aberrant forms of mitochondrial proteins such as the α -subunit. In support of this hypothesis, the truncation we observed was found in isolated mitochondria but lacks the N-terminal 20 kDa of the protein, which includes the MTS. As the MTS is necessary for a protein to be recognised by the translocase of the outer membrane, this suggests that the peptide was truncated after crossing the outer membrane, perhaps at the point of crossing the inner mitochondrial membrane (for a review of mitochondrial import, see Schmidt *et al.*²⁴). The misfolded protein would thus occur in the intermembrane space, where HtrA2 would normally be perfectly placed to degrade it. On the other hand, we find that HtrA2 interacts with the full length α -subunit of the ATP synthase under basal conditions, and the *ATP5A1* gene is transcriptionally upregulated in HtrA2-KO brain, which may indicate a compensatory mechanism. Both these data suggest a specific effect of HtrA2

on the ATP synthase. Further studies will be necessary in order to fully elucidate this mechanism.

In summary, we have characterised the mitochondrial pathology in HtrA2-deficient cells and identified a possible mechanism of neurotoxicity. Our data suggests that loss of HtrA2 leads to severe mitochondrial uncoupling through the ATP synthase, resulting in depletion of cellular ATP. This lack of ATP in turn renders HtrA2-deficient cells significantly more vulnerable to cytotoxicity in response to any further inhibition of mitochondrial respiration, and we propose that it is this vulnerability to ischaemic conditions, which may ultimately cause the neuronal death observed in the HtrA2-deficient mice.

Materials and Methods

Cell culture. HtrA2-knockout mice were generated in-house at Cancer Research UK and have been described previously.² Mixed litters were obtained by crossing heterozygote animals and comparing genotypes within a litter. Animal husbandry and experimental procedures were performed in full compliance with the United Kingdom Animal (Scientific Procedures) Act of 1986. For primary mouse cortical and midbrain cultures, pups were culled between postnatal days P1–3. Cerebral hemispheres or midbrain were removed into sterile eppendorfs containing 1 ml chilled HEPES-buffered salt solution (0.137 M NaCl, 5.4 mM KCl, 0.25 mM Na₂HPO₄, 0.44 mM KH₂PO₄, 1.3 mM CaCl₂, 1.0 mM MgSO₄, 4.2 mM NaHCO₃, pH 7.4). The HEPES-buffered saline solution (HBSS) was then removed and replaced with 1 ml pre-warmed trypsin–EDTA solution for 5 min at room temperature. The cultures were pelleted by centrifugation at 2000 r.p.m. for 5 min, then the trypsin was gently aspirated and the cells washed first in pre-warmed HBSS, then in warm neurobasal medium containing 2% B27 supplement, 2 mM glutamine, 100 IU/ml penicillin and 100 IU/ml streptomycin. The cells were resuspended in 1 ml warm complete neurobasal medium and 3–4 drops of cells were plated per well on poly-L-lysine coated coverslips in 6-well plates (6–8 cover slips per animal). The cultures were incubated in a humidified incubator at 37 °C with 5% CO₂ in air for 3–4 h, then 2 ml pre-warmed neurobasal medium added. Half the medium was replaced after 2 days, after which half the medium was replaced weekly. All live cell imaging experiments were performed between d10–d14 in culture.

Immortalised WT and HtrA2-KO MEFs have been described previously.² Stable HtrA2-knockdown (KD) SH-SY5Y cells were generated by lentiviral infection with shRNA from Open Biosystems (Lafayette, LA, USA; shRNA oligo ID 315866). HEK293T cells stably expressing the TAP tag or C-terminally TAP-tagged HtrA2 have been described previously.²⁵ Immortalised and stable cell lines were cultured in Dulbecco's modified Eagle medium supplemented with foetal calf serum (10%), L-glutamine (5 mM) and sodium pyruvate using standard cell culture technique.

Measurement of $\Delta\Psi_m$. For measurements of $\Delta\Psi_m$, cells plated on 22 mm glass coverslips were loaded for 30 min at room temperature with 25 nM TMRM (Invitrogen, Paisley, UK) in a HBSS composed of 156 mM NaCl, 3 mM KCl, 2 mM MgSO₄, 1.25 mM KH₂PO₄, 2 mM CaCl₂, 10 mM glucose and 10 mM HEPES; pH adjusted to 7.35 with NaOH. The dye remained present in the media at the time of recording. Confocal images were obtained using a Zeiss 710 VIS CLSM (Zeiss, Oberkochen, Germany) equipped with a META detection system and a $\times 40$ oil immersion objective. TMRM was excited using the 560 nm laser line and fluorescence was measured above 580 nm. For basal $\Delta\Psi_m$ measurements, Z-stack images were obtained by confocal microscopy and analysed using Zeiss software (Zeiss). For analysis of response to mitochondrial toxins, images were recorded continuously from a single focal plane. TMRM is used in the redistribution mode to assess $\Delta\Psi_m$, and therefore a reduction in TMRM fluorescence represents mitochondrial depolarisation.

Measurement of NADH/FAD redox index. NADH autofluorescence was measured using an epifluorescence inverted microscope equipped with a $\times 20$ fluorite objective. Excitation light at a wavelength of 350 nm was provided by a Xenon arc lamp, the beam passing through a monochromator (Cairn Research, Faversham, Kent, UK). Emitted fluorescence light was reflected through a 455 nm long-pass filter to a cooled CCD camera (Retiga, QImaging, Surrey, BC, Canada) and digitised to 12 bit resolution. Imaging data were collected and analysed using

software from Andor (Belfast, UK). FAD autofluorescence was monitored using a Zeiss 710 VIS CLSM equipped with a META detection system and a $\times 40$ oil immersion objective. Excitation was measured using the 454 nm Argon laser line and fluorescence was measured from 505 to 550 nm. Illumination intensity was kept to a minimum (at 0.1–0.2% of laser output) to avoid phototoxicity and the pinhole set to give an optical slice of $\sim 2 \mu\text{m}$.

Measurement of oxygen consumption. To measure respiration rate in intact cells, approximately 1×10^7 cells were suspended in respiration medium (HBSS) with 10 mM D-glucose in a Clark-type oxygen electrode thermostatically maintained at 37 °C. The oxygen electrode was calibrated with air-saturated water, assuming 406 nmol O atoms/ml at 37 °C. Oxygen consumption was measured over 10 min with addition of oligomycin (final concentration 2 $\mu\text{g/ml}$) and FCCP, 0.5 μM . All data were obtained using an Oxygraph Plus system (Hansatech Instruments, Norfolk, UK) with chart recording software.

To measure RCR, intact mitochondria were isolated from the brains of WT and HtrA2-KO mice aged P20 by a method of differential centrifugation²⁶ and resuspended in medium containing 135 mM KCl, 10 mM NaCl, 20 mM HEPES, 0.5 mM KH₂PO₄, 1 mM MgCl₂, 5 mM EGTA and 1.86 mM CaCl₂ at pH 7.1. Oxygen consumption was measured in a Clark-type oxygen electrode thermostatically maintained at 25 °C. Glutamate (5 mM) and malate (5 mM) were added to measure Complex I-linked respiration, succinate (5 mM) with rotenone (5 μM) were added to measure Complex II-linked respiration. All data were obtained using an Oxygraph Plus system with chart recording software.

Measurement of mitochondrial ROS. For measurements of mitochondrial ROS, cells were loaded with 5 μM MitoSOX (Molecular Probes, Invitrogen) in HBSS for 10 min at room temperature and washed once with HBSS before recording. MitoSOX fluorescence was then recorded overtime using a Zeiss 710 VIS CLSM, exciting using the 560 nm laser line and measuring above 580 nm. The rate of increase in mitochondrial fluorescence was measured using Zeiss image analysis software (Zeiss).

Kinetic ATP measurements. This was performed as previously described.²⁷ In brief, WT and HtrA2-KO or KD cells transfected with a cytosolic luciferase construct were plated on glass coverslips and placed in a 37 °C heated chamber in a home built luminometer. Cells were constantly perfused with a HEPES balanced salt solution (recipe above) at 37 °C. Luciferin (5 μM for experiments with MEFs, 10 μM for stable HtrA2-KD SH-SY5Ys) was added into this saline, followed by ATP (1 mM). Under these conditions, the light output of a coverslip of transfected cells was in the range of up to 8000 counts/s for each measurement versus a background lower than 150 counts/s. Luminescence was entirely dependent on the presence of luciferin.

Tandem affinity purification. TAP control and HtrA2-TAP cells were lysed in IPP150 lysis buffer (10 mM Tris-Cl pH 8.0, 150 mM NaCl, 2% CHAPS) and incubated with rabbit IgG sepharose beads (Sigma, Poole, UK) for at least 2 h. The beads were washed three times in IPP150 buffer, then bound proteins were removed by cleavage with TEV protease (Invitrogen) for 1.5 h at room temperature in a buffer composed of 10 mM Tris-Cl pH 8.0, 150 mM NaCl, 2% CHAPS, 0.5 mM EDTA and 1 mM DTT. TEV eluate was then diluted in calmodulin binding buffer (10 mM Tris-Cl pH 8.0, 150 mM NaCl, 2% CHAPS, 1 mM Mg-acetate, 1 mM imidazole, 2 mM CaCl₂ and 10 mM β -mercaptoethanol) and incubated with calmodulin affinity resin (Stratagene, Stockport, Cheshire, UK) for 2 h at 4 °C. Finally bound proteins were eluted with calmodulin elution buffer composed of 10 mM Tris-Cl pH 8.0, 150 mM NaCl, 2% CHAPS, 1 mM Mg-acetate, 1 mM imidazole, 2 mM EGTA and 10 mM β -mercaptoethanol. Inputs and eluates were analysed by western blot using antibodies against the ATP synthase α -subunit (Proteintech Group, 1:1000) and HtrA2 (Cell Signaling, 1:4000).

Proteomic analysis. Mitochondria were prepared from the livers of KO and WT animals and purified on Percoll gradients using standard procedures. Mitochondrial samples (150 μg) were resuspended in IEF rehydration buffer (6 M urea, 2 M thiourea, 2% (w/v) CHAPS, 0.5% (w/v) ampholines (pH 3–10) IPG buffer (Amersham Biosciences, Buckinghamshire, UK), 18 mM DTT and a trace amount of bromophenol blue) and run on non-linear IPG strips (pH 3–10, BioRad, Hertfordshire, UK) as previously described.²⁸ For the second SDS-PAGE dimension the IPG strips were incubated for 15 min in an equilibration buffer containing 50 mM Tris-HCl, 6 M urea, 30% glycerol (v/v), 2% SDS (w/v),

bromophenol blue 0.002% (w/v) and 64 mM DTT, pH 8.8. The strips were then given a further 15 min incubation in a modified equilibration buffer in which the DTT was replaced by 135 mM iodoacetamide. The strips were immersed in Tris-glycine buffer and applied to 10% SDS polyacrylamide gels and electrophoresed under standard conditions. Gels were stained with SYPRO ruby and imaged using ProXPRESS proteomic imaging system (Perkin Elmer Life Sciences, Cambridge, UK) and Progenesis Workstation image analysis software (Non-Linear Dynamics, Newcastle, UK). Spots of interest were excised from stained 2D gels using an automated spot picker (ProPic, Perkin Elmer Life Sciences), tryptic digested and analysed on a MALDI ToF mass spectrometer (M@LDI R, Micromass, Manchester, UK) using a mass range of 900–3000 Da as previously described.²⁸ Peptide mass spectrometric data was analysed automatically or manually by ProteinLynx and MASCOT software (Matrix Science Ltd., London, UK), respectively, and protein identity determined by submission to SWISS-PROT and TrEMBL databases.

Quantitative real-time PCR. RNA was extracted from the snap-frozen brains of WT and HtrA2-KO mice aged P30 using the RNeasy RNA extraction kit (Qiagen, Crawley, UK) according to the manufacturer's protocol. cDNA was generated using Superscript III reverse transcriptase (Invitrogen) with oligo(dT) primers. Quantitative PCR was performed using SybrGreen PCR mastermix (BioRad) with primers designed across each exon boundary of ATP5A1 (for primer sequences see Supplementary Table 1). CT values were obtained using the Rotor-Gene 6000 software (Qiagen) and analysed by the $\Delta\Delta CT$ method²⁹ relative to GAPDH expression and WT exon 1 expression.

Measurement of free cytosolic magnesium. For measurements of $[Mg^{2+}]_c$, cells were loaded for 30 min at room temperature with 5 μM Mag-Fura-AM (Molecular Probes, Invitrogen) and 0.005% pluronic acid in HBSS. Mag-Fura fluorescence was monitored in single cells using excitation light provided by a Xenon arc lamp, the beam passing through a monochromator at 340 and 380 nm (Cairn Research). Emitted fluorescence light was reflected through a 515 nm long-pass filter to a cooled CCD camera (Retiga, QImaging) and digitised to 12 bit resolution. All imaging data were collected and analysed using software from Andor. Traces, obtained using the cooled CCD imaging system, are presented as the ratio of excitation at 340 and 380 nm, both with emission at >515 nm.

Whole-body plethysmography. Respiratory rate (f_R , breaths/min) and tidal volume (V_T , ml/kg) were assessed by whole-body plethysmography in conscious mice aged P20 as described previously.^{30,31} The animal was placed in a recording chamber (~ 50 ml), which was flushed continuously with humidified mixture of 79% nitrogen and 21% oxygen at a rate of ~ 200 ml min^{-1} (temperature 22–24 °C). The animals were allowed ~ 15 min to acclimatize to the chamber environment at normoxia/normocapnia (21% O₂, 79% N₂ and $<0.3\%$ CO₂) before measurements of baseline ventilation were taken. Before and after each of the experiment the plethysmograph was calibrated by repeated injections and withdrawal of air (0.05, 0.1 ml) from within the recording chamber. Changes in f_R , V_T and minute ventilation (V_E ; $f_R \times V_T$; ml/min/kg) were averaged and expressed as means \pm S.E.M.

Statistical analysis. Data were generated from a minimum of three independent experiments. Statistical analysis and exponential curve fitting were performed using Origin 7 (OriginLab Corporation, Northampton, MA, USA) software. Unless otherwise described, data were analysed by parametric Student's *t*-tests and significance expressed: * $P < 0.05$, ** $P < 0.01$. Where it was necessary to normalise each experiment to WT in order to eliminate variables between experiments (e.g., kinetic ATP production experiments), a one-sample *t*-test was used to determine significance. For all graphs, error bars represent mean \pm S.E.M.

Conflict of Interest

The authors declare no conflict of interest.

Acknowledgements. HPF is funded by the Medical Research Council (MRC career development award G0700183). VSB is funded by the MRC and Brain Research Trust (BRT). ZY is funded by a Neurotrain Early Stage Research Training Fellowship through the European Union Research Program FP6. KMH and ED are funded by a Wellcome/MRC Parkinson's Disease Consortium grant to UCL/IoN, the University of Sheffield and the MRC Protein Phosphorylation Unit at the University of

Dundee (grant number WT089698). MC is funded by the BBSRC, Central Research Fund, Bloomsbury Colleges Consortium, PetPlan Charity and RVC Internal Funds. KC, VF, NM and LMM are funded by the MRC. NWW is funded by the MRC, PDS and Wellcome Trust. AVG is a Wellcome Trust Senior Research Fellow. AYA is Parkinson's UK Senior Research Fellow. We thank David Brown and Rebekah Jukes for assistance with the mass spectrometric analysis of mitochondrial proteins.

- Vande Walle L, Lamkanfi M, Vandenabeele P. The mitochondrial serine protease HtrA2/Omi: an overview. *Cell Death Differ* 2008; **15**: 453–460.
- Martins LM, Morrison A, Klupsch K, Fedele V, Moiso N, Teismann P *et al*. Neuroprotective role of the Reaper-related serine protease HtrA2/Omi revealed by targeted deletion in mice. *Mol Cell Biol* 2004; **24**: 9848–9862.
- Strauss KM, Martins LM, Plun-Favreau H, Marx FP, Kautzmann S, Berg D *et al*. Loss of function mutations in the gene encoding Omi/HtrA2 in Parkinson's disease. *Hum Mol Genet* 2005; **14**: 2099–2111.
- Bogaerts V, Nuytemans K, Reumers J, Pals P, Engelborghs S, Pickut B *et al*. Genetic variability in the mitochondrial serine protease HTRA2 contributes to risk for Parkinson disease. *Hum Mutat* 2008; **29**: 832–840.
- Kieper N, Holmstrom KM, Ciceri D, Fiesel FC, Wolburg H, Ziviani E *et al*. Modulation of mitochondrial function and morphology by interaction of Omi/HtrA2 with the mitochondrial fusion factor OPA1. *Exp Cell Res* 2010; **316**: 1213–1224.
- Tain LS, Chowdhury RB, Tao RN, Plun-Favreau H, Moiso N, Martins LM *et al*. Drosophila HtrA2 is dispensable for apoptosis but acts downstream of PINK1 independently from Parkin. *Cell Death Differ* 2009; **16**: 1118–1125.
- Nicholls DG, Ferguson SJ, Nicholls DGB. *Bioenergetics 3*. 3rd edn: Academic Press: Amsterdam, London, 2002.
- Ward MW, Rego AC, Frenguelli BG, Nicholls DG. Mitochondrial membrane potential and glutamate excitotoxicity in cultured cerebellar granule cells. *J Neurosci* 2000; **20**: 7208–7219.
- Rego AC, Ward MW, Nicholls DG. Mitochondria control ampa/kainate receptor-induced cytoplasmic calcium deregulation in rat cerebellar granule cells. *J Neurosci* 2001; **21**: 1893–1901.
- Chance B, Williams GR. Respiratory enzymes in oxidative phosphorylation. I. Kinetics of oxygen utilization. *J Biol Chem* 1955; **217**: 383–393.
- Votyakova TV, Reynolds IJ. DeltaPsi(m)-Dependent and -independent production of reactive oxygen species by rat brain mitochondria. *J Neurochem* 2001; **79**: 266–277.
- de Wet JR, Wood KV, DeLuca M, Helinski DR, Subramani S. Firefly luciferase gene: structure and expression in mammalian cells. *Mol Cell Biol* 1987; **7**: 725–737.
- Jouaville LS, Pinton P, Bastianutto C, Rutter GA, Rizzuto R. Regulation of mitochondrial ATP synthesis by calcium: evidence for a long-term metabolic priming. *Proc Natl Acad Sci USA* 1999; **96**: 13807–13812.
- Leysens A, Nowicky AV, Patterson L, Crompton M, Duchon MR. The relationship between mitochondrial state, ATP hydrolysis, $[Mg^{2+}]_i$ and $[Ca^{2+}]_i$ studied in isolated rat cardiomyocytes. *J Physiol* 1996; **496** (Part 1): 111–128.
- Abramov AY, Scorziello A, Duchon MR. Three distinct mechanisms generate oxygen free radicals in neurons and contribute to cell death during anoxia and reoxygenation. *J Neurosci* 2007; **27**: 1129–1138.
- Jones JM, Datta P, Srinivasula SM, Ji W, Gupta S, Zhang Z *et al*. Loss of Omi mitochondrial protease activity causes the neuromuscular disorder of mnd2 mutant mice. *Nature* 2003; **425**: 721–727.
- Scott ID, Nicholls DG. Energy transduction in intact synaptosomes. Influence of plasma-membrane depolarization on the respiration and membrane potential of internal mitochondria determined in situ. *Biochem J* 1980; **186**: 21–33.
- Shin K, Nakamoto RK, Maeda M, Futai M. FOF1-ATPase gamma subunit mutations perturb the coupling between catalysis and transport. *J Biol Chem* 1992; **267**: 20835–20839.
- Zhang Y, Oldenburg M, Fillingame RH. Suppressor mutations in F1 subunit epsilon reouple ATP-driven H⁺ translocation in uncoupled Q42E subunit c mutant of Escherichia coli F1F0 ATP synthase. *J Biol Chem* 1994; **269**: 10221–10224.
- Majander A, Lamminen T, Juvonen V, Aula P, Nikoskelainen E, Savontaus ML *et al*. Mutations in subunit 6 of the F1F0-ATP synthase cause two entirely different diseases. *FEBS Lett* 1997; **412**: 351–354.
- Celotto AM, Frank AC, McGrath SW, Fergestad T, Van Voorhies WA, Buttle KF *et al*. Mitochondrial encephalomyopathy in Drosophila. *J Neurosci* 2006; **26**: 810–820.
- Moiso N, Klupsch K, Fedele V, East P, Sharma S, Renton A *et al*. Mitochondrial dysfunction triggered by loss of HtrA2 results in the activation of a brain-specific transcriptional stress response. *Cell Death Differ* 2009; **16**: 449–464.
- Radke S, Chander H, Schafer P, Meiss G, Kruger R, Schulz JB *et al*. Mitochondrial protein quality control by the proteasome involves ubiquitination and the protease Omi. *J Biol Chem* 2008; **283**: 12681–12685.
- Schmidt O, Pfanner N, Meisinger C. Mitochondrial protein import: from proteomics to functional mechanisms. *Nat Rev Mol Cell Biol* 2010; **11**: 655–667.
- Plun-Favreau H, Klupsch K, Moiso N, Gandhi S, Kjaer S, Frith D *et al*. The mitochondrial protease HtrA2 is regulated by Parkinson's disease-associated kinase PINK1. *Nat Cell Biol* 2007; **9**: 1243–1252.

26. Domijan AM, Abramov AY. Fumonisin B1 inhibits mitochondrial respiration and deregulates calcium homeostasis—implication to mechanism of cell toxicity. *Int J Biochem Cell Biol* 2011; **43**: 897–904.
27. Campanella M, Casswell E, Chong S, Farah Z, Wieckowski MR, Abramov AY *et al*. Regulation of mitochondrial structure and function by the F1Fo-ATPase inhibitor protein, IF1. *Cell Metab* 2008; **8**: 13–25.
28. Twiddy D, Brown DG, Adrain C, Jukes R, Martin SJ, Cohen GM *et al*. Pro-apoptotic proteins released from the mitochondria regulate the protein composition and caspase-processing activity of the native Apaf-1/caspase-9 apoptosome complex. *J Biol Chem* 2004; **279**: 19665–19682.
29. Livak KJ, Schmittgen TD. Analysis of relative gene expression data using real-time quantitative PCR and the 2(-Delta Delta C(T)) method. *Methods* 2001; **25**: 402–408.
30. Rong W, Gourine AV, Cockayne DA, Xiang Z, Ford AP, Spyer KM *et al*. Pivotal role of nucleotide P2 × 2 receptor subunit of the ATP-gated ion channel mediating ventilatory responses to hypoxia. *J Neurosci* 2003; **23**: 11315–11321.
31. Trapp S, Aller MI, Wisden W, Gourine AV. A role for TASK-1 (KCNK3) channels in the chemosensory control of breathing. *J Neurosci* 2008; **28**: 8844–8850.



Cell Death and Disease is an open-access journal published by Nature Publishing Group. This work is licensed under the Creative Commons Attribution-NonCommercial-Share Alike 3.0 Unported License. To view a copy of this license, visit <http://creativecommons.org/licenses/by-nc-sa/3.0/>

Supplementary Information accompanies the paper on Cell Death and Disease website (<http://www.nature.com/cddis>)